RESEARCH ARTICLE

The Development of a Magnesium Biodegradable Stent: Design, Analysis, and Fabrication

Authors

Chenhao Xu[1], Zhangzhang Yin[2,*], Prabir Roy-Chaudhury[3], Begona Campos-Naciff[4], Guangfeng Hou[1], Mark Schulz[1,*]

Affiliations

[1]Department of Mechanical and Materials Engineering, University of Cincinnati, OH 45221 United States
[2]Ecolab Inc., Naperville, IL 60563 United States
[3]UNC Kidney Center, University of North Carolina, Chapel Hill, NC 27599 United States
[4]Inovasc LLC, Cincinnati, OH 45212 United States

***Corresponding authors**:
Z. Yin
yinzg@mail.uc.edu
M. Schulz
schulzmk@ucmail.uc.edu

Abstract

Stents are widely used as scaffolding to open up blood vessel stenosis. A stent can provide early stage scaffolding, increase blood flow, and optimize hemodynamics. Stainless steel is the most popular material for conventional stents, and it has excellent mechanical behavior during deformation. On the downside, stents made of stainless steel remain in the body permanently and may cause complications or lead to occlusion of the vessel. Biodegradable stents that eventually dissolve and disappear in the body are being developed to overcome these shortcomings. However, biodegradable materials such as magnesium alloys are relatively brittle and cannot deform as much as stainless steel. A proper geometry for the stent that allows large displacement and plastic deformation is necessary and required. In this paper, a balloon-expandable design of magnesium AZ31 alloy venous stent is proposed and evaluated. Computational analysis using finite element analysis (FEA) tools simulated the expansion and recoiling process. The stent was expanded from 6.0 mm to 10.0 mm in the radial direction with the expansion ratio of 1.67. Strain and stress distributions, structural stiffness, and radial strength were studied. The maximum stress did not exceed the ultimate tensile strength (in the plastic region) of the stent material, and the maximum strain was 64% of the elongation. The stent design was then fabricated with methods of electro-discharge machining (EDM), laser machining, and electro-polishing. Lastly, these prototyped stents were prepared for future in-vivo experiment in animal models.

Keywords: biodegradable stent, magnesium, finite element analysis

1. Introduction

In 1977, Dr. Andreas Gruentzig created a surgical procedure, angioplasty [1], in which a small inflatable balloon catheter is dilated at the blood vessel blockage [2]. This method - called percutaneous transluminal coronary angioplasty (PTCA) - was a breakthrough but lead to restenosis [3]. Restenosis is the blood vessel healing response after injury and caused by a local vessel's biologic response to the injury [3]. Ultrasonic observations indicate that recoiling was a major cause for restenosis after PTCA [4]. In 1988, the concept of stenting was introduced by Dr. Julio Palmaz to improve the angioplasty procedure [2]. A Stent is a small tubular structure that is implanted in a diseased region of a vessel via a catheter [5]. Providing mechanical scaffolding of damaged blood vessels to restore lumen and flow conditions in these vessels is the major function of stents. The mechanical scaffolding from stents alleviates the vessel recoil and reduces restenosis [3]. On the contrary, due to the long-term pressure on the vessel wall from the stent, neointimal hyperplasia has become a newly created problem resulting in luminal narrowing, i.e. in-stent restenosis. Neointimal hyperplasia describes how the vascular muscle cells proliferate in the tunica initimal which thickens the blood vessel wall and reduces the lumen space. A common solution for in-stent restenosis is implantation of a drug eluting stent. However, a shortcoming of the drug eluting stents is the high rate of late thrombosis and restenosis [6].

The function of stents is often not a long-term sustained requirement in many situations. A stent that can temporary provide scaffolding and disappear after the healing is completed is an alternative solution. Biodegradable materials and biodegradable stents have been emerging fields since the first patent "metallic stent which is degradable in vivo"

in 2002 by Heublein [7]. In the past, biodegradable stents made from polymer, magnesium, and even iron have been tested as alternative stent materials [3]. In 2016, the Food and Drug Administration (FDA) approved the first biodegradable coronary artery stent that was made of polymers [8,9]. However, the low elastic modulus of the material reduced strength of the stent [8,10]. Stents made of iron have also been tested by ARMCO® [11]. Iron stents degraded extremely slowly and did not show significant improvement reducing neointimal hyperplasia [12–14]. Magnesium stents balance the features of degradation rate, strength, and flexibility when compared to iron stents and polymer stents. There are several advantages of biodegradable stents. Similar to conventional stents that remain in the body permanently, degradable stents provide the early stage scaffolding in the target blood vessel to increase its diameter for increased blood flow. Biodegradable stents act as a conduit for the temporary blood vessel remodeling and inhibit neointimal hyperplasia, which reduces patients' risk for late thrombosis from conventional stents [3]. Most importantly, biodegradable stents dissolve and disappear in a certain period which enables the stent to have a higher drug loading and to avoid the long-term use of anti-platelet agents [3]. Platelets are a major component of blood and they enhance wound healing. An anti-platelet agent can reduce the chance of blood clots in vessels.

In the present study, a design for a magnesium biodegradable stent (MBS) is discussed. The design was verified using finite element analysis (FEA) and prototyping stents were fabricated for in-vivo experiment. Instead of a typical arterial stent, this proposed stent was a venous stent and made of AZ31 alloy.

2.   Design of the Biodegradable Stent

2.1.   Stent Features

There are many factors influencing stent design, such as material, structure, application, expansion method, and expansion ratio.

Expansion methods for balloon-expandable and self-expandable stents are directly related to the stent materials. A balloon-expandable stent (plastic strain range stent) requires material with a large plastic region to minimize the elastic deformation. Minor recoiling caused by the elastic deformation is inevitable during the balloon deflation [15]. On the contrary, a self-expandable stent (elastic stent) is manufactured at the expanded state and then compressed into a delivery system such as a tube. The stent springs back to substantially the original geometry when released in the blood vessel [5]. Materials with low elastic modulus and high yield stress that give a large elastic range are preferred [5]. Based on the magnesium alloy material properties, a small elastic region and relatively large plastic region are the characteristics of balloon-expandable stents.

The MBS was targeted to be placed in a vein. Veins have thinner vessel walls and larger lumen diameter than arteries. The larger lumen diameter allows inserting a larger stent than an arterial stent. Thus, the desired stent for a vein will have a larger diameter with a small expansion ratio. In addition, the structure (design of the struts shape and size) is an important design factor. The stent family often can be classified into five categories, coil, helical spiral, woven, individual rings, and sequential rings. Coil and individual ring designs usually are not used for vascular applications [12,15]. Woven structure is often used for a self-expandable stent. Helical spiral stents with great flexibility have no or minimal internal connection points [15]. This type of structure lacks longitudinal strength. The sequential rings design provides the most balanced characteristics among all five categories. It usually consists of wave-shaped struts and connecting elements (bridges) [15]. The strut designs can be further divided into peak-to-peak and peak-to-valley patterns. The connection bridges can be further divided into open-cell and closed-cell structure.

Therefore, the MBS shall be a balloon-expandable stent with a sequential-ring structure. The goal is to expand the stent to 10 mm diameter based on the application.

2.2.   Geometry Design

This section describes the process of designing the MBS. Mechanical stress and strain behaviors are the key features of any stent. Conventional stents usually undergo uneven strain and stress distribution because material such as stainless steel 316L (SS 316L) has the capacity to tolerate large local deformation. A stent made from SS 316L can expand to the target geometry from a few large deformations along the struts. The elongation of SS 316L is approximate 0.5 [16]. However, magnesium stents require a relatively low and uniform concentration of strain and stress due to the low ductility of AZ31 or other Mg alloys. From a design perspective, each segment of the stent would ideally share the plastic deformation to prevent extreme strain and stress concentrations. In other words, strut segments should strain similarly during the expansion.

Struts with small curvature were introduced for the MBS design. A segment with small curvature can distribute stress along the strut and reduce stress concentration during the stent expansion. At the same time, a peak-to-valley structure was selected because it had smaller cell size than a peak-to-peak structure. According to Prabir Roy-Chaudhury, MD, a

smaller cell size is preferred to prevent neointimal hyperplasia.

Figure 1a illustrates a closed-cell structure that has the smallest cell size for the peak-to-peak design. However, the cell size is still one of the largest among all the designs considered in this paper. In addition, this type of design lacks flexibility since bridges connect every internal node on the strut. If the bridges were longer, it would lead to a larger cell size (Figure 1a). If the bridges were shorter or even eliminated, it would lead to increased thickness at each peak area (Figure 1b). As a biodegradable stent, uniform thickness and width is preferred.

(a)

(b)
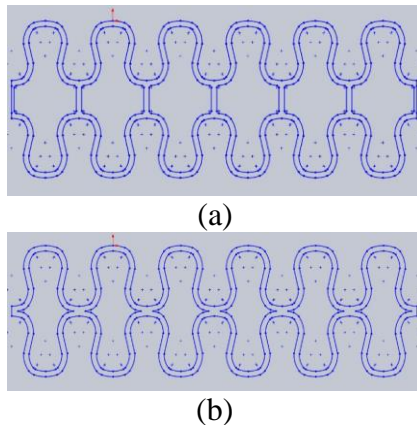
Figure 1. Illustrations of peak-to-peak structures: (a) with long bridge and large cell size; (b) without bridge connection and uniform strut thickness

The next step was the decision of the bridge layout which directly influenced the geometry structure, cell size, mechanical properties, and appearance. Before finalizing the design, there were four types of bridge layouts proposed (Figure 2). In order to calculate the cell size of each type, the inner shadow area of one periodic unit was defined as "1" (Figure 3).
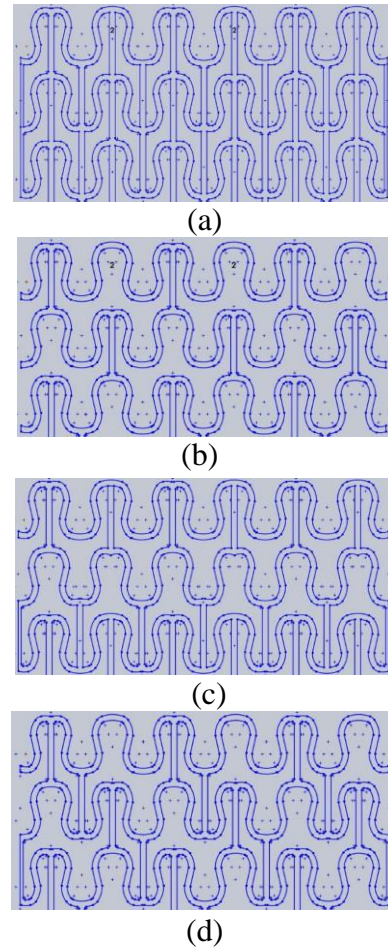

(a)

(b)

(c)

(d)

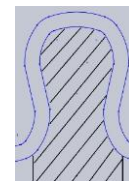**Figure 2.** Four candidates of bridge layout.

Figure 3. The cell size area of "1" in the shadow field.

- Type A (Figure 2a) was a closed-cell design because bridges connect every internal node on the strut. It was the strongest structure but lacks flexibility. The longitudinal length of this design was fixed, which was not applicable in practice. The cell size was 1.0.
- Type B (Figure 2b) was an open-cell structure because there were free-shifting internal nodes on the strut. It had the lowest bridge density and the largest cell

http://journals.ke-i.org/index.php/mra

size of 4.0. Opposite of Type A, this design lacks longitudinal strength. The low bridge density and free-shifting peaks could not ensure the strut unit will uniformly expand during expansion.

- Type C (Figure 2c) was a combination of open-cell and closed-cell structure because the internal nodes were connected to bridges except to the struts on two sides. While the bridge layout was uneven, the cell space is identical with the value of 2.0. The major issue was there are no bridges embedded in every other strut layer, which could cause uneven expansion among strut units in practice.
- Type D (Figure 2d) was also a combination of open-cell and closed-cell structure. It had a diagonal layout of bridges with an average cell size of 2.0. There were two different cell sizes, 1.0 and 3.0. This type of bridge layout was similar to the Lekton Magic stent from Biotronik, Berlin, Germany. In the x-axis direction, bridges were divided into groups of two bridges and inserted at every two peak-to-valley periodic units.

Type A and B were excluded due to lack of either flexibility or strength. Between Type C and D, Type D proposed a balanced design on the aspects of strength, flexibility, bridge density, and cell size.

The MBS model was built in SolidWorks (Dassault System Solidworks Corp., Waltham, MA, US). The stent consisted of three components, crown, bar arm, and bridge (Figure 4a). The crowns and bar arms formed the struts. Instead of a single arc, the crown contained two different components (Figure 4b). This was because pre-angled transitions between arc #1 and #2 allowed the stent to stay in a small diameter at the crimped state and provided a large angle shift during the expansion. The height of the strut was about 2.8 mm and width of each periodical unit was 3.14 mm. The height of the bridge was 3.0 mm. Both the struts and bridges had an identical width of 300 μm.
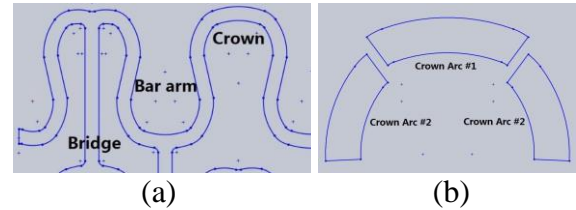

Figure 4. Major components of the MBS: (a) The crown, bar arm, and bridge; (b) detailed layout of the crown.

Figure 5 shows (a) the 2D planar model and (b) the 3D tubular model of a typical MBS. It contained 8 strut layers and each strut layer included 6 periodic units that gave a diameter of 6 mm. The number of periodical units on the strut and the length of stent were customizable. The common stent used in in-vivo experiments had a length of 20 mm with the diameter of 4 or 6 mm.
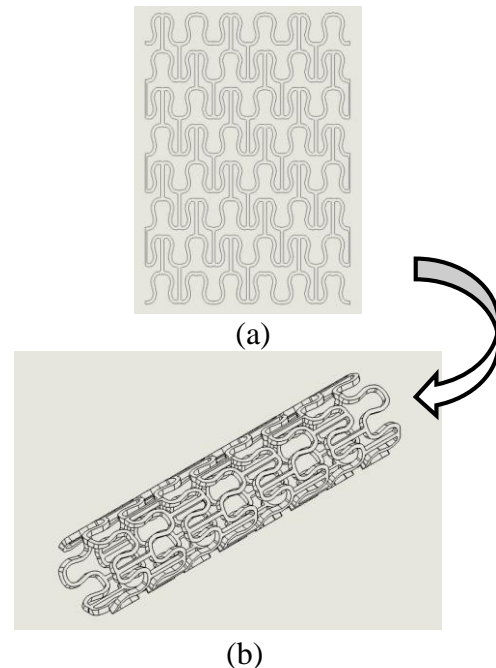

Figure 5. Final design of the MBS in: (a) 2D planar model; and (b) 3D tubular model.

3.   Analysis of Stent Expansion

Computer-aided simulation assists the stent design process. Creating and validating

physical prototypes is an expensive and time-consuming task and it usually doesn't provide sufficient feedback on the mechanics of deformation [2]. Numerical analysis like finite element analysis (FEA) can provide a less costly option and be more efficient for validating complex geometries. The stent model simulation predicts the strain and stress magnitude, distribution and potential fracture area during the expansion and recoiling. The simulation was performed using ABAQUS (Dassault System Simulia Corp., Johnston, RI, US). In order to increase the analysis accuracy, a MBS planar specimen with 2 struts and one third of total length (Figure 6a) and a MBS tubular specimen with 2 entire struts (Figure 6b) were introduced for 2D planar and 3D tubular analyses. Both specimens were imported from SolidWorks to Abaqus.
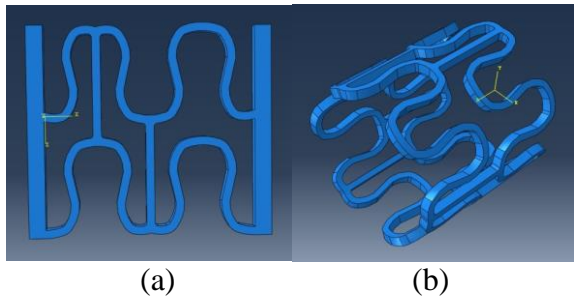

(a)   (b)

Figure 6. The MBS specimen of: (a) 2D planar FEA model; and (b) 3D tubular FEA model.

3.1. Material Properties

Conventional stents are usually made from stainless steel, titanium, or polymers. The AZ31B alloy was considered as a degradable material candidate for the MBS. This kind of alloy usually contains 2.5% – 3.5% of aluminum, 0.7% – 1.3% of Zinc, and a small amount of Manganese. The following table lists the mechanical properties of the AZ31B alloy [16–18].

Table 1. Mechanical Properties of AZ31B Alloy.

Elastic Modulus	Yield Stress	Tensile Stress	Failure Stress
45 GPa	220 MPa	278 MPa	249 MPa
Elongation	Poisson's Ratio		Density
0.16	0.35		1800 Kg/m³

ABAQUS analysis uses the true strain and stress relations. Based on the engineering strain and stress profile, the true strain and stress data can be calculated by the following equation:

$$\epsilon_{tru} = \ln\left(1 + \epsilon_{eng}\right) \text{ (Equation 1)}$$

$$\sigma_{tru} = \sigma_{eng}\left(1 + \epsilon_{eng}\right) \text{ (Equation 2)}$$

Where ε represents the strain and σ represents the stress.

Based on Equation 1 and 2, the true failure stress is 289 MPa and the corresponding strain is 0.15.

3.2. Evaluation of a Planar Stent Specimen

Stiffness is an important determinant of the mechanical performance of a stent. The 2D planar specimen was analyzed using FEA. In order to maintain the identical and uniform expansion rate on the MBS specimen, two rectangular and solid boundary bars were added to the both sides of the specimen (Figure 6a). The MBS had an initial diameter of 6 mm and was expected to expand to 10 mm. The circumference of the stent at an initial state was 18.84 mm and the expanded circumference would be 31.42 mm. The stent specimen was required to expand to one third of the difference of 31.42 mm and 18.84 mm, which was 4.19 mm. The analysis included one step and was performed in ABAQUS/Standard. The specimen was

meshed using a 3D stress element C3D8R with element size of 0.07 mm. The first boundary condition fixed all six degrees of freedom on the face parallel to YZ-plane of the left boundary bar. The second boundary condition only allowed the corresponding face of the right boundary bar to move in X-axis with a displacement of 4.19 mm.

Assume the mechanical behavior of a periodic unit acts like a spring that follows Hook's law (Equation 3). The planar strut in Figure 6a then can be also considered as a spring. The struts in the planar stent result in a parallel combination of spring. In the situation of a 2 by 2 stent specimen (Figure 6a), there are two parallel struts. Each strut contains two periodic units and each periodic unit consists of two identical curves against each other. Assume the stiffness coefficient of each identical curve is k. The Hook's law is represented by the following equation,

$$\boldsymbol{k} = \frac{d\boldsymbol{F}}{d\boldsymbol{x}} \text{ (Equation 3)}$$

Where k represents the stiffness coefficient, F represents the net force applied, and x represents the displacement.

The sum of stiffness coefficients in series is $\boldsymbol{Ks} = \frac{\boldsymbol{k1 \ x \ k2}}{\boldsymbol{k1 + k2}}$ (Equation 4) and the sum of stiffness coefficients in parallel is $\boldsymbol{Kp} = \boldsymbol{k1 + k2}$ (Equation 5), where k_1 and k_2 represent the coefficients of identical curves in the periodic unit. According to Equation 3 and 4, the stiffness coefficient of one periodic unit is k/2 and the stiffness coefficient of one strut is k/4. Therefore, the stiffness coefficient of the planar specimen is:

$$\boldsymbol{K} = \frac{\boldsymbol{k}}{\boldsymbol{4}} + \frac{\boldsymbol{k}}{\boldsymbol{4}} = \frac{\boldsymbol{k}}{\boldsymbol{2}}$$

The stiffness coefficient of the planar specimen will be calculated by Equation 3.

The applied net force and the displacement of the specimen will be recorded during the expansion.

3.3. Evaluation of a Tubular Stent Specimen

The second FEA model was built for analyzing the strain and stress distribution, recoil ratio, and radial strength during the balloon inflation and deflation. Similar to the planar analysis, it also used the ABAQUS/Standard method with the same element type and element size. The tubular analysis, based on cylindrical coordinates, included 2 steps, balloon inflation (expansion) and balloon dilation (recoiling). The balloon model was created in ABAQUS and assembled with the MBS specimen (Figure 7). It was meshed as a shell surface, element type SFM3D4.
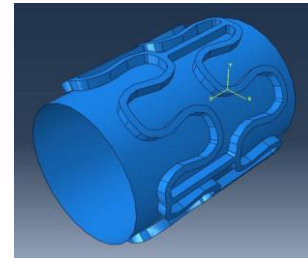

Figure 7. The assembled FEA models of the balloon and the MBS specimen in the tubular analysis.

During the expansion step, the nodes on the balloon were commanded to shift 2 mm along the positive R-axis while the remaining 5 degrees of freedom were fixed. The MBS specimen was expected to expand to 10.0 mm in diameter at the end of this step. During the recoiling step, the balloon recovered back to initial state to allow the stent to recoil. Between the stent and the rigid surface of balloon, a surface-to-surface contact feature was applied with a friction coefficient of 0.1. The recoiling ratio was calculated as [19]:

$$\boldsymbol{R} = \frac{d_{inflated} - d_{deflated}}{d_{inflated}} \boldsymbol{100}\% \text{ (Equation 6)}$$

Where d represents the diameter of the stent.

At the same time, a MBS prototyped sample made from AZ31B alloy was compared to the FEA results. Studies indicate that commercial coronary stents often fail to achieve the recoiling ratio of 11% – 23% [20]. Slotted-tube stents (closed-cell design) usually have good performance with recoiling ratios of 8% – 9% [20]. Due to the lack of information about venous stent, the recoiling ratio of the MBS was compared to commercial coronary stents.

Besides, the radial strength is another important factor when describing a stent design. The radial strength was calculated by the total radial reaction force applied on the outer surface of MBS during the re-crimping process. The mechanical behavior of MBS included two regions, elastic and plastic regions. The elastic region could be very short due to the residual stress after recoiling. When entering the plastic region, the radial reaction force was expected to increase, which was similar to the expansion process. The radial strength was defined by a linear y = mx + b function with an offset of 0.1 mm parallel to another linear function whose slope is based on the initial linear behavior of the reaction force [8]. The intersection of the linear function y = mx + b and the original reaction force function defined the radial strength of the MBS.

3.4.   Analysis Results

The displacements at the (a) initial and (b) expanded stages of the planar analysis are shown in Figure 8. Nodes on the right end of the specimen had displacements of 4.19 mm at the expanded stage. Figure 9 displays the stress and strain distribution results of the planar analysis. The Von Mises and plastic strain intensity (PEEQ) were used to evaluate the results. Von Mises stress was calculated by the following equation:

$$\sigma_v^2 = \frac{1}{2}\left[(\sigma_{11} - \sigma_{22})^2 + (\sigma_{22} - \sigma_{33})^2 \right.$$
$$\left. + (\sigma_{33} - \sigma_{11})^2 + 6(\sigma_{12}^2 + \sigma_{23}^2 + \sigma_{31}^2)\right]$$
(Equation 7)

The largest stress was 282 MPa located at the inner curve of strut valley (Figure 9) and the largest plastic strain was 0.111. During the expansion, concentrated stress and strain gained on the upper and lower surface of the strut. The inner surface of the strut curve underwent tension while the outer surface underwent compression.
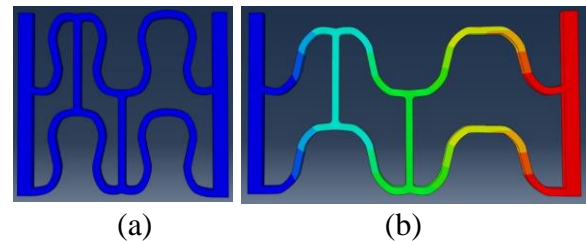

(a)   (b)

Figure 8. The 2D planar analysis results with the respect of displacement: (a) the initial state; and (b) the expanded state
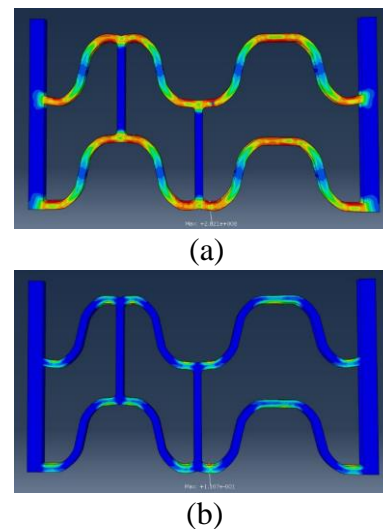

(a)

(b)

Figure 9. The 2D planar analysis results with the respect of: (a) Von Mises; and (b) strain magnitude at the expanded state.

The stress first grew in the linear elastic region and then entered the non-linear plastic region. The pulling force (Figure 10a) can be

calculated from the left end of the rectangular boundary. The stiffness coefficient K represents the derivative of the pulling force and the displacement of each strut unit (Figure 10b). Due to the feature of the linear elastic region, the stiffness coefficient remained a constant of 1.36 N/mm in the figure. The length of the constant value indicated the expansion length in elastic region, which was 0.575 mm. After entering the plastic deformation region, the value of stiffness coefficient K trended to converge to 0.11 N/mm.
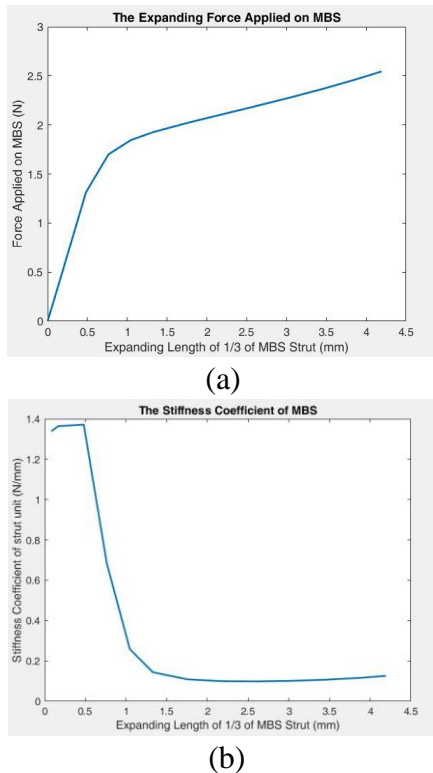

(a)

(b)

Figure 10. The 2D planar analysis results with the respect of: (a) expanding force applied on the specimen; and (b) stiffness coefficient of the specimen during the expansion process.

In the tubular analysis, the full process of expansion and recoiling was analyzed. The MBS specimen was expanded by inflating a balloon and then the stent recoiled after the balloon was deflated. Figures 11 and 12

illustrate the stress and strain distributions at initial, expanded, and recoiled stages. The largest Von Mises and plastic strain reached 279 MPa and 0.096 located at the inner curve of strut valley. The maximum strain was only 64% of the elongation of AZ31 alloy. Compared to the results of the planar and tubular analyses, the maximum value of stress and strain and the location in the tubular analysis matched the results in the planar analysis. However, the stress concentration in the tubular analysis seemed closer to the surface of the struts. This may be caused by the pure tension applied on the planar model while the tubular model was expanded by a balloon. After the balloon deflation and stent recoiling, the highest Von Mises dropped to 220 MPa and the plastic strain remained at 0.096.
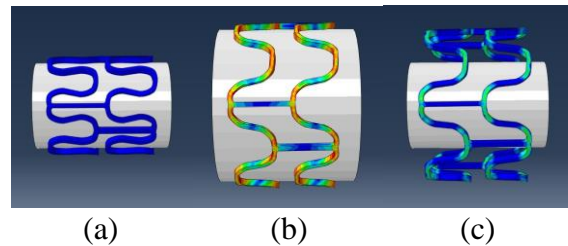

(a)   (b)   (c)

Figure 11. The 3D tubular analysis results with the respect of Von Mises at: (a) the initial state (b) the expanded state; and (c) the recoiled state.
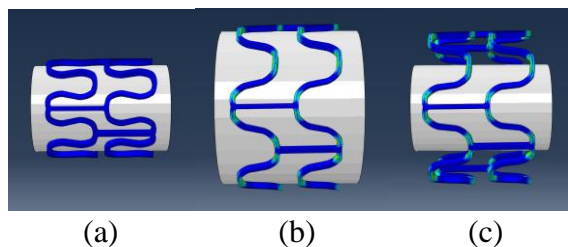

(a)   (b)   (c)

Figure 12. The 3D tubular analysis results with the respect of strain magnitude at: (a) the initial state; (b) the expanded state; and (c) the recoiled state.

Figure 13 (a – c) demonstrates the radial displacement at (a) initial, (b) expanded, and

(c) recoiled stages. Figure 13d shows the recoiled stage of an actual MBS that made of magnesium AZ31 alloy. The MBS specimen increased from a diameter of 6.0 mm to 10.0 mm, and then recoiled to 9.47 mm. The difference of diameter changes before and after recoiling was 0.53 mm, equivalent to the planar displacement of 1.67 mm. During the expansion step, the stent specimen started to enter the plastic deformation at the radial displacement of 0.26 mm, equivalent to the planar displacement of 1.63 mm. Since the recoiling was also caused by the elastic deformation, it is necessary to evaluate the difference in percentage of both displacements. The recoiled displacement was 2.5% larger than the linear elastic displacement, which was a very small error percentage. The recoiling ratio based on the simulation was 5.27%. The actual MBS bench test showed the recoiled diameter of 9.52 mm and the recoiling ratio based on the testing was 4.80%. The error percentage of the simulation result was 0.53%. Therefore, the bench test result validated the accuracy of the MBS structural analysis.
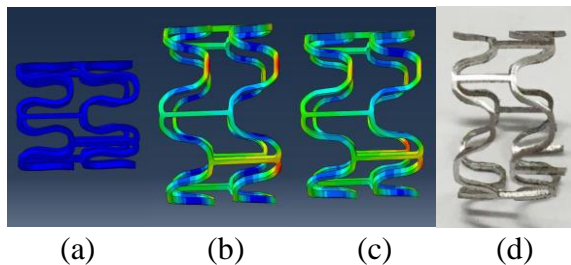

(a)   (b)   (c)   (d)

Figure 13. The 3D tubular analysis results with the respect of radial displacement at: (a) the initial state; (b) the expanded state; (c) the recoiled state to compare with; (d) the radial displacement at recoiled state of the actual stent.

Besides the strain/stress distribution and recoiling ratio, the radial strength is another important parameter for the design a stent. In order to obtain the radial strength, the force reaction from the stent outer surface when crimping the stent must be calculated. The radial behavior during the crimping of the MBS is shown in Figure 14. The stent specimen started to crimp at the diameter of 9.47 mm. The slope of the elastic region was -2.5. The radial strength of MBS was 1.45 N/mm when it's expanded to 10 mm with the expansion ratio of 1.67. Compared to an arterial stent with the similar structure, the radial strength was 0.69 N/mm when the expansion ratio was 1.64 [8]. The venous MBS had a stronger structure compared to an arterial stent with a similar expansion ratio.
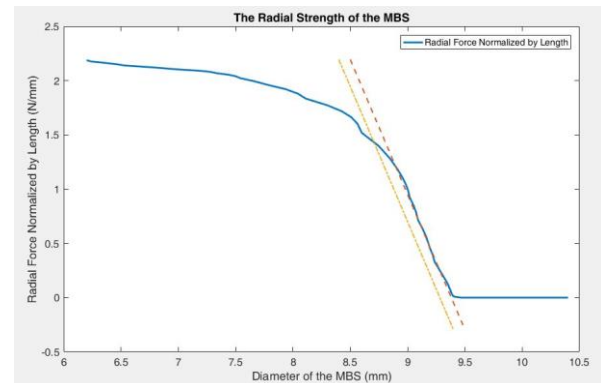

Figure 14. The 3D tubular analysis results with the respect of radial strength when the MBS specimen was expanded to the diameter of 10.0 mm.

4. Prototyping

4.1. Tube Machining and Laser cutting

The quality of stent fabrication directly impacts the accomplishment of design requirements. It is an important link between the design and applications. The MBS fabrication steps were followed by tubing machining, laser cutting, and post-processing (electro polishing). The tubing was machined using electro-discharge machining (EDM) of

a commercial AZ31B alloy. Each tube required two cutting procedures, the inner and outer circumferences. The outer and inner diameters of the tube were 6 mm and 5.2 mm. The wall thickness was 0.4 mm. Figure 15 shows the AZ31 alloy tube machined by EDM before laser cutting. The laser cutting engraved the stent strut geometries on the tube according to the MBS drawings from an AutoCAD file. Material irradiated by the laser was vaporized due to the high energy and temperature. The laser cutting of Mg process was done by InoTech Laser Corp. in California, US. The strut cross section was designed to be larger than the actual requirement to allow for any adjustments in the post processing of the stent. The strut cross sectional width and height was expected to be 300 μm by 400 μm after the laser machining.
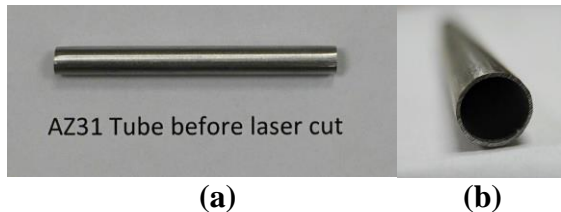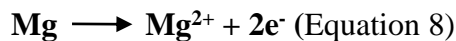

(a)   **(b)**

Figure 15. The product of the tubing machining by EDM: (a) top view; and (b) front view.

4.2.   Post Process (Electro polishing)

The electro polishing procedure removed burrs caused by laser machining, adjusted the strut geometries, and polished the stent surface. The mechanism of electro polishing followed the chemical equation:

$$Mg \longrightarrow Mg^{2+} + 2e^- \text{ (Equation 8)}$$

Magnesium is ionized to magnesium ions in the electrolyte. The stent was the anode while a carbon rod was the cathode. During the treatment, the geometries of the strut cross section decreased to 250 μm by 350 μm. At the same time, the MBS surface obtained a

smoother finish (Figure 16). Figure 16 demonstrates an expanded MBS. The stents before and after the electro polishing treatment were compared under a benchtop SEM. Figure 17(a – b) and Figure 17(c – d) represent the states before and after the treatment. The left-hand side figures (a and c) were magnified 200 times and right-hand side figures (b and d) were magnified 150 times. Burrs and chips on the edges were removed. In addition, the strut surface after the electro polishing was smoother. The MBS was then ready for sterilization and in-vivo testing in animal models.
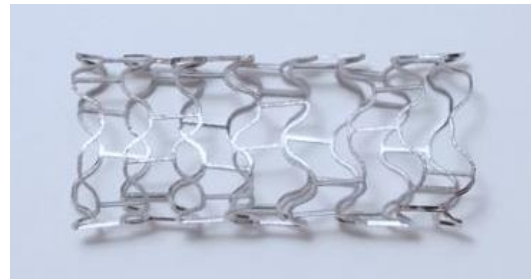

Figure 16. The MBS after electro polishing.

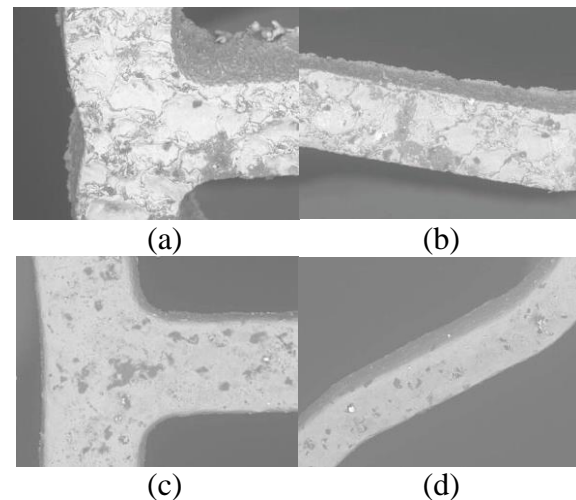(a)   (b)

(c)   (d)

Figure 17. Benchtop SEM photos of the MBS before and after electro polishing. Before electro polishing with: (a) 200 times; and (b) 150 times magnification. Post electro polishing with: (c) 200 times; and (d) 150 times magnification.

5. Conclusions

In the present study, the MBS achieved the preliminary goals of proper geometries, expansion ratio, stable structure, and degradation. The study had three major steps, (1) design, (2) verification, and (3) prototyping. The first step required an appropriate structure that allowed expansion in veins without mechanical failure of the stent. A sequential ring peak-to-valley structure was introduced. Stent struts used a small curvature design that was expected to reduce local stress and strain concentrations. The FEA verified the proposed design. It provided details on strain and stress distribution, recoil ratio, and radial strength. Based on the magnesium AZ31 alloy material properties, the MBS was expected to safely expand and remain in the blood vessel. At a diameter of 10.0 mm, the largest strain was 64% of the elongation. The MBS had a recoiling ratio of 5.27% based on the FEA result and 4.80% based on the actual stent bench test. With the error of 0.53%, it provided strong confidence in the accuracy of the analysis from ABAQUS. In addition, the radial stiffness of the MBS was 1.45 N/mm when the expansion ratio was 1.67. Compared to the arterial stent with a similar structure and similar expansion ratio, the MBS had greater radial strength than the arterial stent. The prototyping was an important link between the design stage and in-vivo or clinical testing stage of the development. All tubes made by EDM met the requirements of 6.0 mm outer diameter and 0.4 mm wall thickness. The electro polishing readjusted the strut geometries and improved the surface finish of the product after laser machining. Future in-vivo animal experiments will evaluate the MBS on the basic stent functions on scaffolding of blood vessels, blood flow enhancement, and the degradation behavior. The MBS behavior in animals will also be compared to conventional permanent stents.

http://journals.ke-i.org/index.php/mra

References

1. Gruentzig AR. Percutaneous transluminal coronary angioplasty. *Semin Roentgentol.* 1981; 16: 152-3.

2. Gay M, Zhang L, Liu WK. Stent modeling using immersed finite element method. *Comput. Methods Appl. Mech. Eng.* 2006; 195: 4358-4370.

3. Waksman R, Pakala R. Biodegradable and bioabsorbable stent. Cardiovascular research institute. *Current Pharmaceutical Design.* 2010, 16, 4041-4051.

4. Mintz GS, Popma JJ, Pichard AD, et al. Arterial remodeling after coronary angioplasty: A serial intravascular ultrasound study. *Circulation.* 1996 Jul 1; 94(1): 35-43.

5. Zahora J, Bezrouk A, Hanus J. Models of stent – comparison and applications. *Physiol. Res.* 56 (Suppl. 1): S115-121, 2007.

6. Kawaguchi R, Angiolillo DJ, Futamatsu H, Suzuki N, Bass TA, Costa MA. Stent thrombosis in the era of drug eluting stents. *Minerva Cardioangiol.* 2007; 55: 199-211.

7. Heublein B, Rohde R, Kaese V, Niemeyer M, Hartung W, Haverich A. Biocorrosion of metallic alloys: a new principle in cardiovascular implant technology? *Heart* 2003; 89, 651-656.

8. Wang Q, Fang G, Zhao YH, Zhou J. Improvement of mechanical performance of bioresorbable magnesium alloy coronary artery stent through stent pattern redesign. *Appl. Sci.* 2018, 8, 2461.

9. Geller J. Food and drug administration approves plethora of medical devices. *J. Clin. Eng.* 2017, 42, 4–10.

10. Giacchi G, Ortega-Paz L, Brugaletta S, Ishida K, Sabaté M. Bioresorbable vascular scaffolds technology: current use and future developments. *Med. Devices.* 2016, 9, 185.

11. Moravej M, Mantovani D. Biodegradable metals for cardiovascular stent application: interests and new opportunities. *Int. J. Mol. Sci.* 2011; 12, 4250-4270.

12. Xu C. Design and simulation of a magnesium based biodegradable stent for hemodialysis application. *Electronic Thesis or Dissertation. University of Cincinnati, 2015.* https://etd.ohiolink.edu/!etd.send_file?accession=ucin1445342007&disposition=inline. Accessed June 19, 2020.

13. Peuster M, Wohlsein P, Brugmann M, et al. A novel approach to temporary stenting: degradable cardiovascular stents produced from corrodible metal-results 6-19 months after implantation into New Zealand white rabbits. *Heart.* 2001; 86, 563-569.

14. Peuster M, Hesse C, Schloo T, Fink C, Beerbaum P, von Schnakenburg C. Long-term biocompatibility of a corrodible peripheral iron stent in the porcine descending aorta. *Biomaterials.* 2006; 27, 4955-4962.

15. Stoeckel D, Bonsignore C, Duda S. A survey of stent designs. *Min Invas. Ther. Allied Technol.* 2002; 11: 137-147.

16. Wu W, Petrini L, Gastaldi D, Villa T, Vedani M. Finite element shape optimization for biodegradable magnesium alloy stents. *Ann. Biomed. Eng.* 2010; 38(9): 2829-40.

17. Gastald D, Sassi V, Petrini L, Vedani M, Trasatti S, Migliavacca F. Contiuum damage model for bioresorbable magnesium alloy devices – application to coronary stents. *J. Mech. Behav. Biomed. Mater.* 2011; 4: 352-365.

18. Avedesian MM, Baker H, eds. *ASM specialty handbook: magnesium and magnesium alloys.* Materials Park, OH. ASM International; 1999.

19. Liang DK, Yang DZ, Qi M, Wang WQ. Finite element analysis of the implantation of a balloon-expandable stent in a stenosed artery. *International Journal of Cardiology.* 2005; 104: 314-318.

20. Carrozza JP, Hosley SE, Cohen DJ, Baim DS. In vivo assessment of stent expansion and recoil in normal porcine coronary arteries differential outcome by stent design. *Circulation.* 1999; 100: 756–760.